VII International Conference on Particle-Based Methods
PARTICLES 2021
P. Wriggers, M. Bischoff, E. Oñate, M. Bischoff, A. Düster & T. Zohdi (Eds)

STRESS ANALYSIS OF SOIL BENEATH WHEEL FOR PLANETARY ROVER BY USING DISCRETE ELEMENT METHOD

Shoko Ono[1,2], Roy Lichtenheldt[2] and Kazuya Yoshida[1]

[1] Department of Aerospace Engineering, Graduate School of Engineering
Tohoku University
Aoba 6-6-01, Sendai, Miyagi 980-8579, Japan
e-mail: shoko.ono.p5@dc.tohoku.ac.jp, yoshida.astro@tohoku.ac.jp

[2] Institute of System Dynamics and Control,
German Aerospace Center (DLR)
Münchener Straße 20, 82234, Weßling, Germany
email: shoko.ono@dlr.de, roy.lichtenheldt@dlr.de

Key words: Discrete Element Method, Planetary Rover, Wheel-Soil Interaction, Soil Flow, Stress Distribution

Abstract. Modeling the interaction between rover's wheel and soft terrain is of great importance in predicting or evaluating wheel performance for lunar and planetary rovers. The current wheel-soil interaction models predict or evaluate wheel performance under certain conditions. However, most of them do not consider the soil flow and deformation, and thus, they cannot capture the physical phenomena of wheel-soil interaction. Developing a new model that includes such physical phenomena contributes to the improvement of prediction accuracy. To develop such a model, it is necessary to analyze soil flow and deformation beneath the wheel. This study analyzes the stress distributions in the soil and soil flow fields beneath the grouser wheel by performing experiments using the discrete element method (DEM) with the particle simulation tool "Sir partsival". In addition to the single wheel simulation, two simple test simulations - an angle of repose test and a shear test - are performed to confirm the soil flow fields and stress distributions in the soil. In the field of fluid dynamics, (shear) stress generally exists along high gradients of flow velocity. These two tests confirm if the soil stress shows the same trend. The wheel simulations are performed under several slip conditions to investigate their influences on soil flow characteristics. The shape of the soil flow region - the shape of the slip line - can be divided into two patterns depending on the slip conditions. The stress increases along the slip line in all simulations. The findings of this study contribute to understanding the relationship between soil velocity field and stress distribution in the soil.

1 INTRODUCTION

Modeling the interaction between rover's wheels and soft terrain is still a big challenge and of great importance in evaluating the wheel performance of a planetary rover. A classical terramechanics model based on the pressure-sinkage relationship, which was introduced by Bekker, has been commonly used for wheel-soil interaction problems for heavy vehicles [1]. Several studies extended the classical model to lightweight vehicles, and the wheel-soil interaction models predict or evaluate wheel performance under certain conditions [2, 3]. However, most of them do not consider the soil flow and deformation, and thus, they cannot capture the physical phenomena of wheel-soil interaction. Developing a new model that includes such physical phenomena contributes to the improvement of the prediction accuracy. To address the issue, it is necessary to analyze and understand soil flow and deformation beneath the wheel.

Several studies experimentally visualized the soil flow fields beneath a grouser wheel based on computer vision techniques such as particle image velocimetry (PIV) [4]. Moreland et al. [5] observed the soil shearing behavior underneath the wheel with grousers and without grousers. They concluded that the grouser wheel can reduce the motion resistance compared to the non-grouser wheel. In our previous research, we analyzed soil flow beneath the grouser wheel on different types of soils and concluded that the soil properties like the shear strength highly affect the soil flowing characteristics [6, 7].

Numerical simulation approaches such as a discrete element method (DEM) have also been widely applied to wheel-soil interaction [8]. The DEM could capture a large soil deformation and a soil flowing behavior at the particle level since this technique discretizes soil as particles. Some researchers have employed the DEM simulation to visualize soil flowing and force fields beneath a wheel. Nakashima et al. [9], for example., described soil flow field beneath the grouser wheels on the sloped terrain. Ravula et al. [10] visualized forces generated on the particles underneath a grouser wheel. They concluded that the wheel sinkage increases with an increase in force concentrations inside the granular soil.

The relationship between soil flow fields and stress distributions is not fully understood, and the soil stress distribution under different wheel traveling conditions are also not predictable. Furthermore, the DEM simulations used for soil flow and force analysis in the past, have not been validated in terms of the soil flow and deformation. Thus, the validity of the soil motion observed in DEM previously is uncertain.

This study analyzes the stress distributions in the soil and soil flow fields beneath the grouser wheel by using the validated DEM simulation. In addition to the single wheel simulations, two simple test simulations - an angle of repose test and a shear test - are performed to confirm the soil flow fields and stress distributions in the soil. Then, the wheel simulations are carried out under several slippage conditions to investigate their influences on the soil flow and stress distributions. The results are discussed from the viewpoint of wheel sinkage, soil flowing velocity, and stress in the soil.

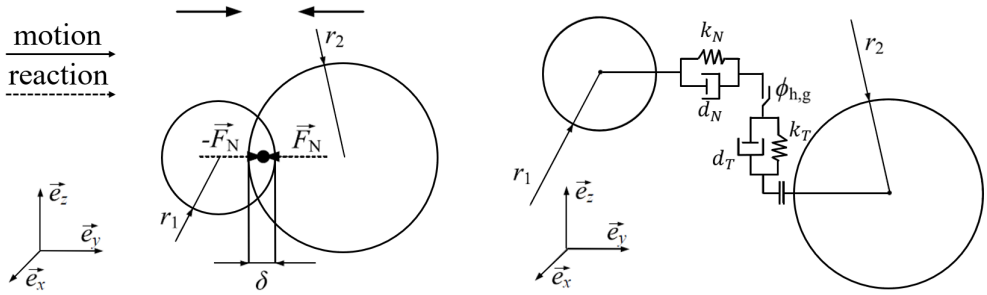

Figure 1: Contact model for DEM [14]

2 DEM SIMULATION

This section introduces a particle-based simulation technique known as a discrete element method (DEM), which was first introduced by CUNDALL and STRACK [11]. This technique has been commonly applied to various dynamical problems in the fields of powder mechanics, soil dynamics, as well as terramechanics. In this study, "Sir partsival", which is a framework for the DEM developed at German Aerospace Center (DLR), is used for the analysis of the wheel-soil interaction [12]. This framework uses a GPU parallized implementation allowing for fast computations and it has already been validated in the previous studies [13].

2.1 DEM Basics

The motion dynamics of particles can be computed based on NEWTON and EULER equations in the DEM. The contact forces acting on each particle, which are typically modeled by springs, viscous dampers, and a slider for considering the friction between particles, are first calculated to determine the particle motion. The contact model for two-particles contact is illustrated in Fig. 1. The contact force in the normal direction $\vec{F}_N^{ij}$ between two particles i and j is computed based on HERTZIAN contact law [14]:

$$\vec{F}_N^{ij} = \left(\frac{2E}{3(1-\nu^2)} \sqrt{r_C^{ij} |\vec{\delta}^{ij}|^3} \right) \vec{n}_c^i + d_{Nmin}^{ij} \dot{\vec{\delta}}^{ij} \tag{1}$$

where E is the Young's modulus, ν is the Poisson's ratio, r_C^{ij} is the mean particle radius, $\vec{\delta}^{ij}$ is the inter-particle overlap in the normal direction, $\vec{n}_c^i$ is the contact normal vector, and d_{Nmin}^{ij} is the normal damping factor, respectively.

In the tangential direction, stick-slip friction is implemented by utilizing a regularized COULOMB friction model. As sticking features elastic deformations in reality, a KELVIN element is used to regularize this state. The resulting tangential force is computed as follows [14]:

$$\vec{F}_{cT}^{ij} = k_T^{ij} \cdot \vec{\delta}_T^{ij} \cdot \text{sign}(\vec{\delta}_T^{ij} \cdot \dot{\vec{\delta}}_T^{ij}) + d_T^{ij} \cdot \dot{\vec{\delta}}_T^{ij} \tag{2}$$

$$\vec{F}_T^{ij} = \begin{cases} \vec{F}_{cT}^{ij} & |\vec{F}_{cT}^{ij}| \leq |\vec{F}_N^{ij}| \cdot \tan(\phi_h) \ \wedge \ |\dot{\vec{\delta}}_T^{ij}| \leq v_{Tmin}^{ij} \\ \vec{F}_N^{ij} \cdot \tan(\phi_g) \cdot (\dot{\vec{\delta}}_T^{ij})_0 & |\vec{F}_{cT}^{ij}| > |\vec{F}_N^{ij}| \cdot \tan(\phi_h) \ \vee \ |\dot{\vec{\delta}}_T^{ij}| > v_{Tmin}^{ij} \end{cases}$$

where k_{T} is the tangential stiffness, d_{T} is the tangential damping coefficient, $\vec{\delta}_{\mathrm{T}}^{ij}$ is the tangential displacement, and ϕ_{g} and ϕ_{h} are slipping and sticking angle of friction, respectively.

The particles in the DEM are commonly modeled as spherical elements due to computational efficiency. On the other hand, real grains generally consists of a high number of edges, and the angular shape becomes a rolling resistance. Hence, a rolling resistance model, which is introduced in [15], is applied to the DEM simulation to reproduce the rolling behavior of real grains.

The partsival used an implicit integration scheme for the realization of more stable and faster simulations. Implicit schemes are commonly implemented as predictor-corrector algorithms. This requires a repeated contact detection and a renewed force calculation in the corrector loop and leads to sacrificing computational performance. In partsival, a force-predictive LICHTENHELDT-jolt-BEEMAN scheme is employed to omit these repeated contact detection and renewed force calculation steps [16].

To better understand the soil behavior, the stress acting on a particle is calculated in post processing as the following equation:

$$\sigma = F/A = ma/A = \rho V a/A \tag{3}$$

F is the forces acting on a particle, A is the cross-section of the center of a particle, m is the particle mass, a is the acceleration of a particle, ρ is a particle density, and V is a particle volume. At first, the particle acceleration is calculated based on the particle velocity at the different two consecutive time steps. Then, the force and stress acting on a particle are computed.

2.2 Particle Parameters for DEM

A two-dimensional (2D) DEM simulation for the single wheel tests was developed and validated in terms of soil deformation in our previous study [17]. The 2D-DEM with spherical particles is realized by limiting the degrees of freedom of each particle. The degree of freedom of each particle is limited to two translational degrees of freedom and

Table 1: Particle parameters for the DEM simulation

Name	Symbol	Value	Unit
particle radius	r	1.5-2.5 (uniform distribution)	[mm]
Young's modulus	E	5.0×10^7	[Pa]
Poisson ratio	ν	0.17	[-]
particle density	ρ	2700	[kg/m^3]
inter-particle friction angle for sliding	ϕ_{g}	25.0	[°]
inter-particle friction angle for sticking	ϕ_{h}	27.0	[°]
rolling resistance coefficient	-	0.9	[-]
inter-particle cohesion	c	0.0	[N/m^2]

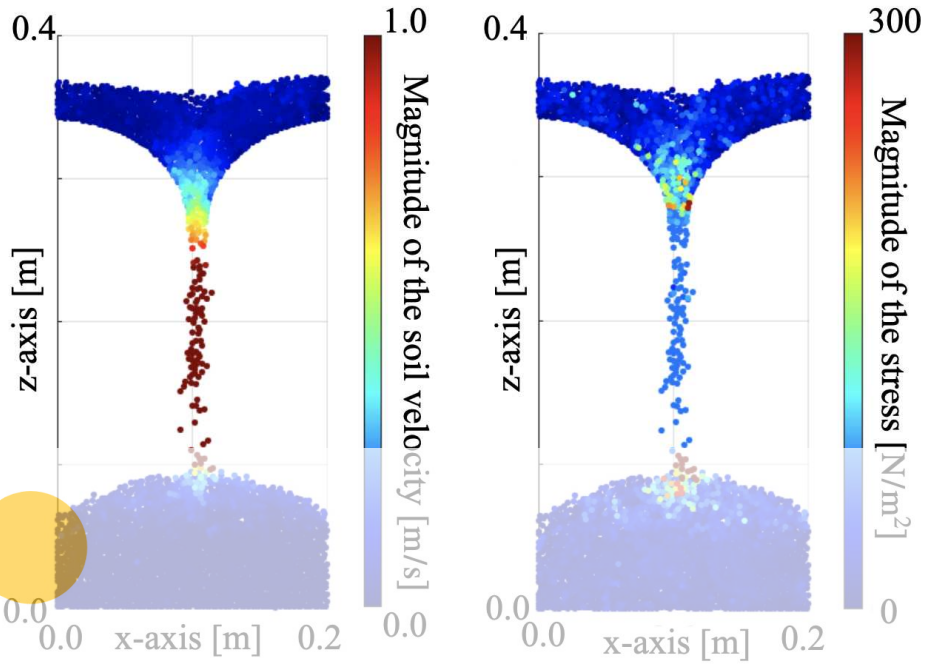

Figure 2: Funnel piling simulation: soil velocity field (left), stress distribution (right)

one rotation degree of freedom, for a total of three degrees of freedom.

The particle parameters used for the simulation in this study are listed in Table 1. These parameters determined based on the properties of Toyoura standard sand, whose characteristics are a nearly homogeneous grain size and lack of cohesion [7]. The particle parameters are divided into three types: material properties, estimation parameters, and tuning parameters. The material properties such as particle density and cohesion were determined based on the real soil properties. The estimation parameters such as Young's modulus and particle radius were calculated by the empirical equations in [14]. The others like friction angle and coefficient of rolling resistance were the tuning parameters. The simulations were performed with the Earth gravitational condition.

3 SIMPLE TEST SIMULATIONS

In this section, the soil flow fields and stress distributions in the soil are discussed by performing the two simple experiments: angle of repose and shear tests. The shear stress generally increases along the high gradients in flow velocity in the field of fluid dynamics. Hence, we confirm if this phenomenon is observed soil mechanics as well.

3.1 Angle of Repose Experiment

The angle of repose test is generally conducted to measure the angle of repose of the sandpile. The procedure of the test is divided into three steps. At first, all particles were set on the top of the virtual test device like a hourglass. Then, the particles fell through the hourglass by gravity. Finally, the sandpile was formed on the bottom of the virtual

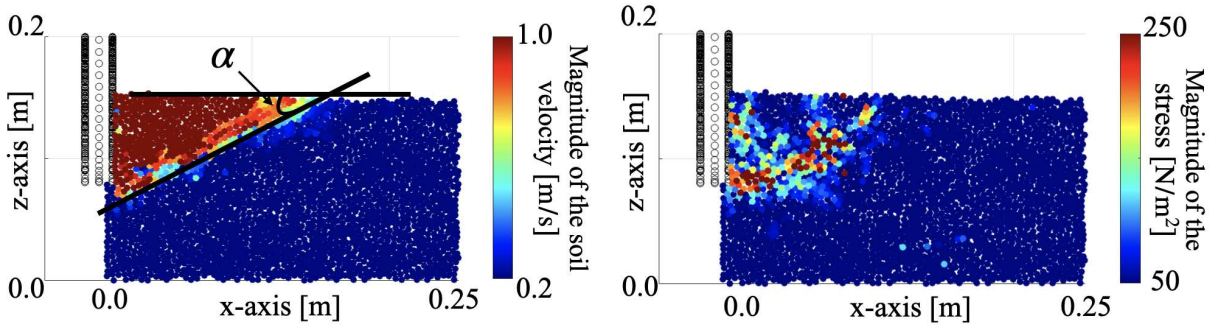

Figure 3: Shear test simulation: soil velocity field (left), stress distribution (right)

device.

The result of the test is shown in Fig. 2. The left figure shows the magnitude of the soil particle velocity, and the right figure shows the magnitude of the stress acting on each particle. A higher velocity is observed when the particles are falling. Following that region, the high velocity is observed around the top of the sandpile. This is because the particles on the top of the sandpile obtain kinetic energy from the falling particles. The other region where shows a higher velocity is above the gap of the hourglass. In this region, the particles start to get pushed towards the funnel and the particles accelerate.

A higher stress region is observed around the top of the sandpile. This is because the particles on the top of the sandpile received a force from the falling particles. Furthermore, the other region where higher stress is observed is above the gap of the hourglass, where shows the gradients in the soil flow velocity. This result indicates that the stress in the soil shows the same trend with that in the fluid dynamics.

3.2 Shear Test

The shear test is commonly applied to investigate the shear characteristics of the soil. The procedure of the shear test is divided into three steps: the preparation of the sandbox, the set of the plate, and finally the plate movement. The plate moves along the x-axis from left to right with a constant velocity of 0.1 m/s.

Fig. 3 illustrates the result of the shear test (left: soil flow velocity field, right: stress inside the soil). When the plate pushes the soil forward, two dedicated regions can be observed. One region is moving with the plate as well as a stationary below. The slip line divides these two regions. This line is observed from the bottom tip of the plate to the soil surface. This slip line is confirmed in a previous study [18]. The angle of the slip line α is also a key parameter, showing the soil characteristics since the internal friction angle is calculated from the angle of slip line as the following equation:

$$45 - \phi/2 = \alpha \tag{4}$$

where ϕ is the internal friction angle. The internal friction angle is generally known to be almost the same as the angle of repose. From our previous laboratory test, the angle of repose of Toyoura sand is 36° [7]. The angle of slip line measured from the image in this

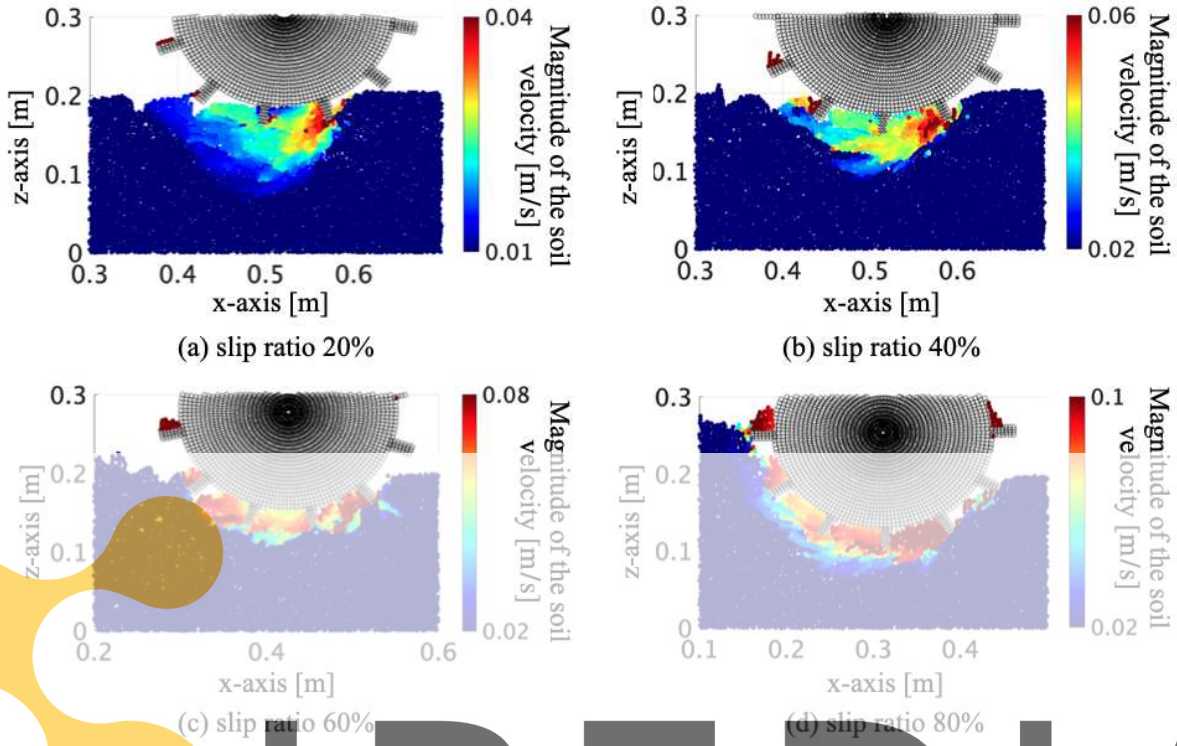

(a) slip ratio 20% (b) slip ratio 40%

(c) slip ratio 60% (d) slip ratio 80%

Figure 4: Single wheel simulations: soil flow velocity fields (slip ratio 20%, 40%, 60%, 80%)

study is 27°, and thus, the internal friction angle calculated from above equation is 36°. Therefore, the angle of slip line is reasonable and this is an additional validation of the DEM simulation.

A higher stress region is concentrated along the slip line. This is because the shear stress increases in the region where the high gradients in soil velocity. High stress is also observed in the vicinity of the plate since the normal stress received from the plate becomes large. In the two simple test simulations, we conclude that the stress increases in the regions with high gradients of flow velocity like the fluid dynamics.

4 SINGLE WHEEL SIMULATIONS

The single wheel simulations are performed to analyze the soil flow fields and stress distributions beneath the grouser wheel. The virtual sandbox, which was filled in with 12,955 particles, had a length of 1.0 m and a height of 0.25 m, respectively. In the lateral, y, direction, only a single particle layer exists. The wheel used for the simulations had a radius of 125 mm and 12 parallel grousers, which were a length of 25 mm and a thickness of 10 mm. The vertical load of the wheel is 80 N. The simulations were carried out under fixed slip conditions: slip ratio of 20, 40, 60, and 80%. The wheel was controlled to keep a constant angular velocity of 0.8 rad/s. The traveling velocity was determined to be a desired slip ratio. In all conditions, the wheel travels along with the x axis from the left to right on the soil surface. The procedure of the simulation divides mainly into three steps:

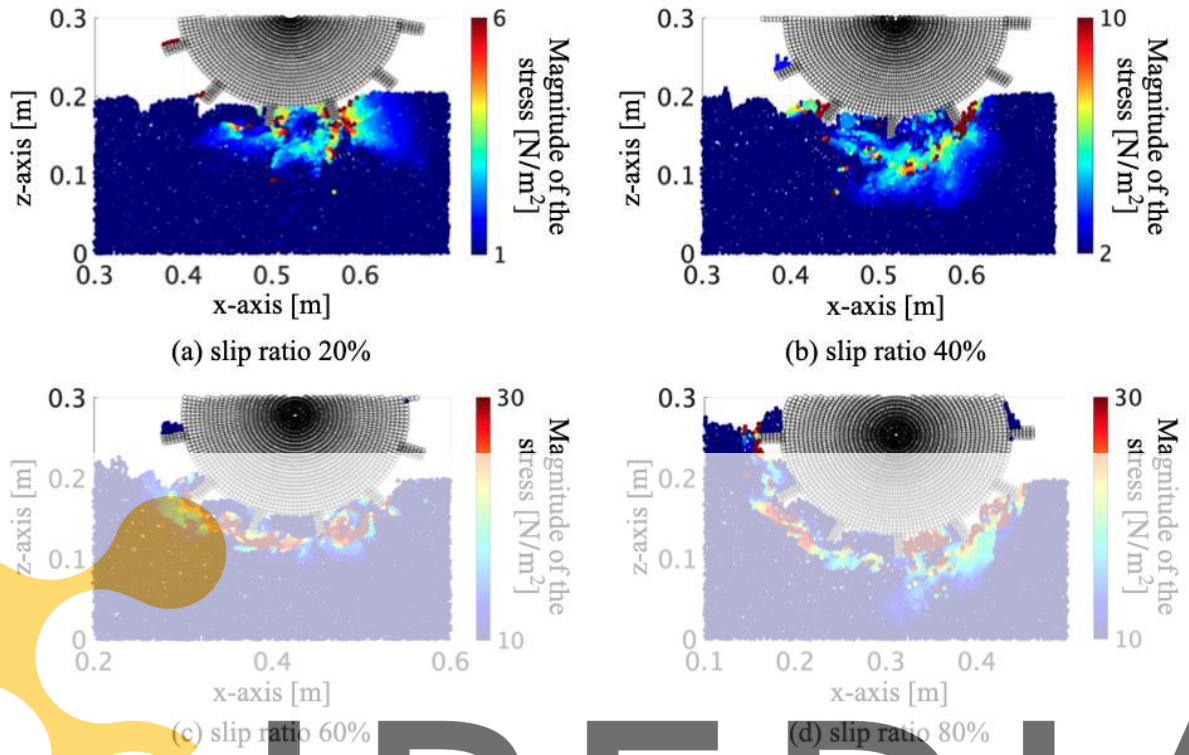

Figure 5: Single wheel simulations: soil stress distributions (slip ratio 20%, 40%, 60%, 80%)

1) the sandbox was first prepared to be stable. 2) the top surface of the sandbed was cut to prepare the flat surface. 3) The wheel was put on the soil surface, and it started rotating with a constant angular velocity.

Fig. 4 shows the soil flow velocity fields beneath the grouser wheel under several wheel slip conditions. The figure shows that the wheel sinkage increases with an increase in the slip ratio as generally observed in laboratory tests. The soil flowing velocity increases with an increase in the wheel slippage. This is because the relative velocity, which is the subtraction of the horizontal velocity of the wheel from rotational velocity, increases with an increase in the slippage.

The shape of the soil flow velocity fields - the shape of the slip line - also depends on the slip ratio. When the wheel slippage is small (slip ratio of 20 and 40%), the soil flows in a parabolic manner from the grouser surface. In the case of the high-slip conditions (slip ratio of 60 and 80%), the soil flows along with the motion trajectory of the grouser, and the grousers dig up more soil. This phenomenon has also been observed in the past experimental study [19], and this is an additional validation for the DEM under different slip conditions. The reason for this difference in the soil flowing shape has not been clarified yet, so further investigation is required for future studies.

The results of the stress in the soil are shown in Fig. 5. The magnitude of the stress also tends to increase as the slip ratio increases, similar to the soil velocity. Regarding the stress distribution, a region where a large stress concentrates can be observed around the slip line under all conditions. This result shows the same trend as the simple test

simulations. In the low slip ratio (20 and 40%), there is a region where shows the high stress caused by grousers with traction. As the result, two trends can be observed. First, as expected from the simple simulations, the stress concentrates along the lines of high-velocity gradients. Second, the stress magnitude is related to the slip ratio.

5 CONCLUSIONS

In this study, we presented and discussed the results of three experiments, angle of repose test, shear test and single wheel test, by using the DEM simulation. From this we conclude three major observations:

- The shape of the soil flow field beneath the grouser wheel depends on the slip conditions. At high slip the soil flows along with the grouser's motion trajectory, whereas at low slip the soil flow propagates from the grouser tip in a parabolic shape.
- The stress magnitude of the soil increases with an increase in the wheel slippage. The highest stress is concentrated around the slip line in all slip conditions.
- As the relationship between the soil flow and stress state, the stress concentrates along high gradients in the soil flow velocity.

This paper contributed to understanding the relationship between wheel slip, soil flow and soil stress. In future studies, the shape of the velocity and stress distributions beneath the grouser wheel are discussed in detail, focusing on the slip angle and angle of the stress distributions. Furthermore, the soil flow field and stress distribution will be investigated using different types of soil like a cohesive soil known as a lunar regolith simulant.

REFERENCES

[1] Bekker, M.G. Introduction to terrain-vehicle systems. University of Michigan Press, Ann Arbor (1969).

[2] Ishigami, G., Miwa, A., Nagatani, K., and Yoshida, K. Terramechanics-based model for steering manuever of planetary exploration rovers on loose soil. *Journal of Field Robotics*, 24 (3), 233–250 (2007).

[3] Irani, R.A., Bauer, R.J., and Warkentin, A. A dynamic terramechanics model for small lightweight vehicles with rigid wheels and grousers operating in sandy soil. *Journal of Terramechanics*, 48, 307-318 (2011).

[4] Moreland, S., Skonieczny, K., Wettergreen, D., Creager, C., and Asnani, V. Soil motion analysis system for examining wheel-soil shearing. In: *17th International Conference of the International Society for Terrain-Vehicle Systems* (2011).

[5] Moreland, S., Skonieczny, K., Inotsume, H., and Wettergreen, D. Soil behavior of wheels grousers for planetary rovers. In: *IEEE Aerospace Conference* (2012).

[6] Ono, S., Namikawa, S. , and Yoshida, K. Analysis of soil deformation and wheel traction on loose terrain using PIV. In: *IEEE Aerospace Conference* (2020).

[7] Ono, S., Namikawa, S., and Yoshida, K. Analysis of soil flow and traction mechanics for lunar rovers over different types of soils using particle image velocimetry. *Journal of Terramechanics* 95, 89-100 (2021).

[8] Nakanishi, R., Nakashima, H., Miyasaka, J., and Ohdoi, K. Tractive performance analysis of a lugged wheel by open-source 3D DEM software. *Journal of Terramechanics* 92, 51-65 (2020).

[9] Nakashima, H., Fujii, H., Oida, A., Momozu, M., Kanamori, H., et al. Discrete element method analysis of single wheel performance for a small lunar rover on sloped terrain. *Journal of Terramechanics* 47, 307-321 (2010).

[10] Ravula, P., Acar, G., and Balachandran, B. Discrete element method-based studies on dynamic interactions of a lugged wheel with granular media. *Journal of Terramechanics* 94, 49-62 (2021).

[11] Cundall, P.A. and Strack, O.D.L.: A discrete numerical model for granular assemblies. *Géotechnique* 29 (1), 47-65 (1979).

[12] Lichtenheldt, R., Kerler, S., Angerer, A., and Reif, W. partsival - Collision-based particle and many-body simulations on GPUs for planetary exploration systems. In: *5th Joint International Conference on Multibody System Dynamics* (2018).

[13] Lichtenheldt, R., Ono, S., and Stubbig, L. Large scale discrete element simulation comparing simulated and real soils in particular. In: *14th World Congress on Computational Mechanics (WCCM) ECCOMAS Congress* (2020).

[14] Lichtenheldt, R. A novel systematic method to estimate the contact parameters of particles in discrete element simulations of soil. In: *IV International Conference on Particle-based Methods - Fundamentals and Applications PARTICLES* (2015).

[15] Obermayr, M., Vrettos, C., Eberhard, P., and Dauwel, T. A discrete element model and its experimental validation for the prediction of draft forces in cohesive soil. *Journal of Terramechanics* 53, 93-104 (2014).

[16] Lichtenheldt, R. A stable, implicit time integration scheme for discrete element method and contact problems in dynamics. In: *V International Conference on Particle-based Methods - Fundamentals and Applications PARTICLES* (2017).

[17] Ono, S., Lichtenheldt, R., and Yoshida, K. Soil flow analysis for planetary rovers based on particle image velocimetry and discrete element method. In: *20th International Conference of the International Society for Terrain-Vehicle Systems* (2020).

[18] Coetzee, C.J. Discrete and continuum modelling of soil cutting. *Computational Particle Mechanics* 1, 409–423 (2014).

[19] Nakamura, H., Nagaoka, K., and Yoshida, K. Soil flow analysis for grouser wheels based on a particle image velocimetry. *Journal of Terramechanics* 91, 233-241 (2020).